Interfaces and Free Boundaries **6** (2004), 295–314

Modeling and simulation of sublimation growth of SiC bulk single crystals[†]

OLAF KLEIN[‡], PETER PHILIP[§], AND JÜRGEN SPREKELS[¶]
Weierstrass Institute for Applied Analysis and Stochastics, Mohrenstrasse 39, D-10117 Berlin, Germany

[Received 28 May 2003]

We present a transient mathematical model for the sublimation growth of silicon carbide (SiC) single crystals by the physical vapor transport (PVT) method. The model of the gas phase consists of balance equations for mass, momentum, and energy, as well as reaction-diffusion equations. Due to physical and chemical reactions, the gas phase is encompassed by free boundaries. Nonlinear heat transport equations are considered in the various solid components of the growth system. Discontinuous and nonlocal interface conditions are formulated to account for temperature steps between gas and solid as well as for diffuse-gray radiative heat transfer between cavity surfaces. An axisymmetric induction heating model is devised using a magnetic scalar potential. For a nonlinear evolution problem arising from the model, a finite volume scheme is stated, followed by a discrete existence and uniqueness result. We conclude by presenting and analyzing results of transient numerical experiments relevant to the physical growth process.

Keywords: Modeling; SiC single crystal; physical vapor transport; diffuse-gray radiation; nonlocal interface conditions; finite volume scheme; numerical solution.

2000 Mathematics Subject Classification: 80A20, 80M25, 65M99, 35K60, 47J35.

1. Introduction

Due to its advantageous physical properties, silicon carbide (SiC) is used in numerous industrial applications. As a semiconductor substrate material, SiC is utilized in electronic and optoelectronic devices such as MESFETs, MOSFETs, thyristors, P-i-N diodes, Schottky diodes, blue and green LEDs, lasers, and sensors. Its chemical and thermal stability enables SiC to be used in high-temperature applications as well as in intensive-radiation environments. Moreover, SiC is especially suitable for usage in high-power and high-frequency applications.

The industrial use of SiC requires the availability of large-diameter, low-defect SiC boules. Moreover, a high growth rate during the production process is desirable to reduce production time and costs. Even though there has been substantial progress in SiC manufacturing in recent years, satisfying all of the aforementioned demands remains challenging, as only partial solutions exist (cf. e.g. [2, 7, 15]).

[†] This work has been supported by the DFG research center "Mathematics for key technologies" (FZT 86) in Berlin and by the German Federal Ministry for Education and Research (BMBF) within the program "Neue Mathematische Verfahren in Industrie und Dienstleistungen" ("New Mathematical Methods in Manufacturing and Service Industry") # 03SPM3B5.

[‡] Email: klein@wias-berlin.de

[§] Email: philip@wias-berlin.de

[¶] Email: sprekels@wias-berlin.de (corresponding author)

We consider the production of SiC single crystals by sublimation growth via *physical vapor transport* (PVT) (modified Lely method, see e.g. [13]). Typically, modern PVT growth systems consist of an induction-heated graphite crucible containing polycrystalline SiC source powder and a single-crystalline SiC seed (see Fig. 1). The source powder is placed in the hot zone of the growth apparatus, whereas the seed crystal is cooled by means of a blind hole, establishing a temperature difference between source and seed.

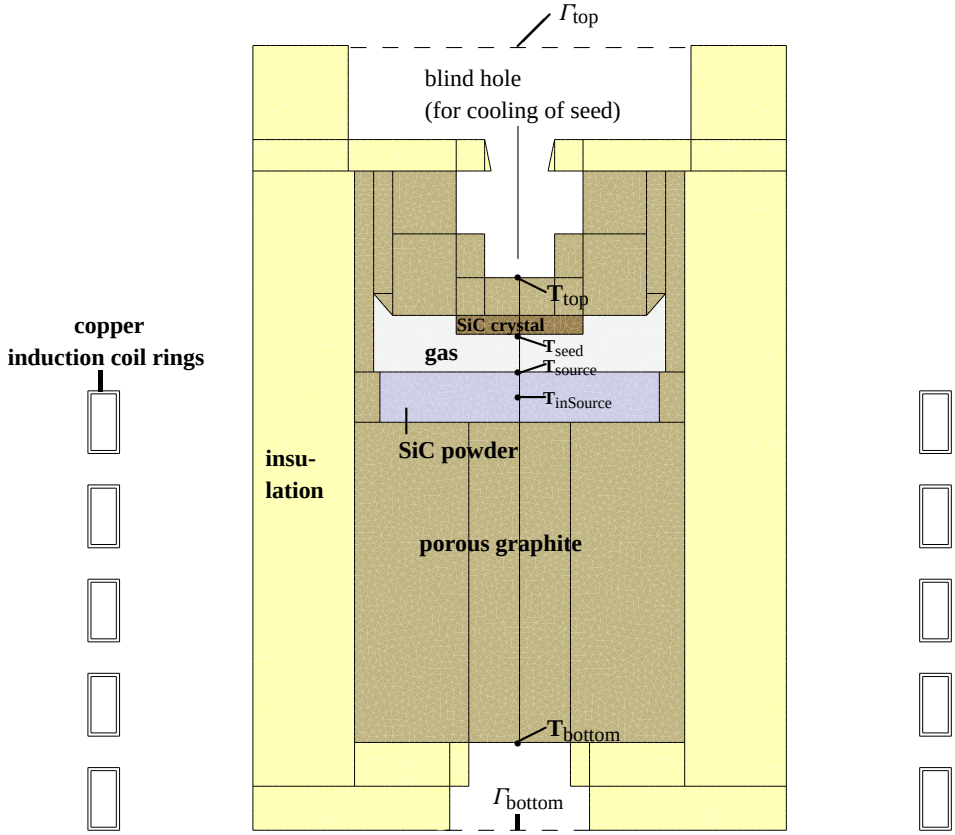

FIG. 1. Setup of growth apparatus according to [17, Fig. 2].

To eliminate contaminants such as S, B, and metallic elements from the growth system in a first heating stage, the apparatus is degassed at some 10^{-3} Pa and heated to about 1200 K. After this contaminant bakeout phase has been completed, a high-purity argon atmosphere is established at 10^5 Pa, and the temperature is further increased. At growth temperature, which can reach up to 3000 K for growth of the SiC polytype 6H, pressure is reduced to about $2 \cdot 10^3$ Pa [1].

After growth temperature has been reached, the SiC source is kept at a higher temperature than the cooled SiC seed, such that sublimation is encouraged at the source and crystallization is encouraged at the seed, causing the partial pressures of Si, Si_2C, and SiC_2 to be higher in the neighborhood of the source and lower in the neighborhood of the seed. As the system tries to equalize the partial pressures, source material is transported to the seed which grows into the reaction chamber.

As the crystal's quality and growth rate depend strongly on the evolution of the temperature distribution [19, 20], mass transport, and species concentrations [21], control of these quantities is essential. However, due to the high temperatures, experimental verification of the correlation between the quantities to be regulated and control parameters such as apparatus configuration, heating power, and argon pressure is extremely difficult and costly.

Thus, theoretical modeling and numerical simulation play a fundamental role in gaining understanding of the relation between control parameters and favorable growth conditions. In consequence, the development of numerical models and software and their application to PVT growth of SiC crystals has been an active field of research in recent years. Recent papers on stationary models include [9, 17]. Transient numerical results concerning the heat transfer during PVT are considered in [3, 11, 16].

The paper is organized as follows: Section 2 covers the mathematical modeling of the process, namely, the gas phase in Section 2.1, the free boundaries in Section 2.2, heat conduction in the solid components in Section 2.3, interface and boundary conditions in Section 2.4, diffuse-gray radiation in Section 2.5, and induction heating in Section 2.6. In Section 3, we consider numerical solutions for the temperature evolution problem, formulating a finite volume scheme in Section 3.1, followed by a discrete existence and uniqueness result (Theorem 1). Finally, in Section 3.2, we discuss numerical results and their implications for the growth process.

2. Mathematical model

2.1 *Gas phase*

Our model of the gas phase is based on continuous mixture theory and Fick's law. Neglecting radiative contributions inside the gas phase, this leads to the following system (2.1), consisting of balance equations for mass, momentum, and energy, as well as reaction-diffusion equations (see [16, Section 2.1] for a detailed derivation):

- Mass Balance:
$$\frac{\partial \rho_{\text{gas}}}{\partial t} + \operatorname{div}(\rho_{\text{gas}} \mathbf{v}_{\text{gas}}) = 0, \tag{2.1a}$$
- Momentum Balance:
$$\frac{\partial (\rho_{\text{gas}} \mathbf{v}_{\text{gas}})}{\partial t} + \operatorname{div}(p_{\text{gas}} \mathbf{1}) = \rho_{\text{gas}} \mathbf{g}, \tag{2.1b}$$
- Energy Balance:
$$\frac{\partial}{\partial t}(\rho_{\text{gas}} \varepsilon_{\text{gas}}) + \operatorname{div}(\rho_{\text{gas}} \varepsilon_{\text{gas}} \mathbf{v}_{\text{gas}} + \mathbf{q}_{\text{gas}} + p_{\text{gas}} \mathbf{v}_{\text{gas}}) = \rho_{\text{gas}} \mathbf{g} \bullet \mathbf{v}_{\text{gas}}, \tag{2.1c}$$
- Reaction-Diffusion Equations (one for each gas species α, $\alpha \in \{\text{Ar, Si, Si}_2\text{C, SiC}_2\}$):
$$\frac{\mathrm{d}c^{(\alpha)}}{\mathrm{d}t} - \frac{1}{\rho_{\text{gas}}} \operatorname{div}(\rho_{\text{gas}} c^{(\alpha)} (D^{(\alpha)})^{-1} (\nabla p^{(\alpha)} - c^{(\alpha)} \nabla p_{\text{gas}})) = \frac{1}{\rho_{\text{gas}}} \rho^{*(\alpha)}, \tag{2.1d}$$

where

$$\frac{\mathrm{d}}{\mathrm{d}t} := \frac{\partial}{\partial t} + \mathbf{v}_{\text{gas}} \bullet \nabla, \tag{2.2a}$$

$$p_{\text{gas}} = \sum_{\alpha} p^{(\alpha)}, \qquad \varepsilon_{\text{gas}} = \sum_{\alpha} c^{(\alpha)} \varepsilon^{(\alpha)}, \tag{2.2b}$$

$$\mathbf{q}_{\text{gas}} = -\kappa_{\text{gas}} \nabla T_{\text{gas}} - \sum_{\alpha} (\rho_{\text{gas}} c^{(\alpha)} \varepsilon^{(\alpha)} + p^{(\alpha)}) (D^{(\alpha)})^{-1} (\nabla p^{(\alpha)} - c^{(\alpha)} \nabla p_{\text{gas}}). \tag{2.2c}$$

In (2.1) and (2.2), the subscript "gas" is used for quantities in the gas mixture, whereas superscripts (α) indicate quantities in the gas species α. The meaning of the symbols is as follows:

ρ_{gas} – mass density,
t – time,
$\mathbf{v}_{\text{gas}}$ – local mean velocity of gas molecules,
$\mathbf{1}$ – unit matrix,
p_{gas} – total pressure,
$p^{(\alpha)}$ – partial pressure,
$\mathbf{g}$ – gravimetric acceleration,
ε_{gas} – total internal energy,
$\varepsilon^{(\alpha)}$ – partial internal energy,
$\mathbf{q}_{\text{gas}}$ – heat flux,
$c^{(\alpha)}$ – mass concentration,
$D^{(\alpha)}$ – diffusion coefficient,
$\rho^{*(\alpha)}$ – partial mass source (chemical reactions, phase transitions),
κ_{gas} – thermal conductivity,
T_{gas} – absolute temperature.

Furthermore, Equations (2.1) are coupled through the following material laws, furnished by the theory of ideal gases:

$$p^{(\alpha)} = \rho_{\text{gas}} c^{(\alpha)} \frac{R}{M^{(\alpha)}} T_{\text{gas}}, \qquad \varepsilon^{(\alpha)} = z^{(\alpha)} \frac{R}{M^{(\alpha)}} T_{\text{gas}}, \tag{2.3a}$$

$$\rho^{*(\alpha)} = \sum_{i=1}^{N} \gamma_i^{(\alpha)} M^{(\alpha)} \mu_{\text{H}} \Lambda^{(i)} \tag{2.3b}$$

for each gas species α, where R is the universal gas constant, $M^{(\alpha)}$ is the molecular mass, $z^{(\alpha)} = 3/2$ for single-, $z^{(\alpha)} = 5/2$ for double-, and $z^{(\alpha)} = 3$ for multi-atomic gas molecules, N is the number of chemical reactions and phase transitions, $\gamma_i^{(\alpha)}$ are the stoichiometric coefficients, μ_{H} is the hydrogen molecular mass, and $\Lambda^{(i)}$ are rates of chemical reactions or phase transitions, respectively.

The unknown quantities in the above equations are

$$\{\rho_{\text{gas}}, \mathbf{v}_{\text{gas}}, c^{(\alpha_1)}, \ldots, c^{(\alpha_A)}, T_{\text{gas}}\}, \tag{2.4}$$

where A is the number of gas species considered, i.e. $A = 4$ in the case considered above. For each time instant, the state of the gas mixture is determined by the $A + 3$ quantities in (2.4).

While, for temperatures above 2500 K, Si, Si_2C, and SiC_2 make up a significant portion of the gas mixture, for lower temperatures only Ar is present, and, for higher temperatures, heat is mainly transported via radiation. So, e.g. for the simulations of the temperature distribution and its evolution considered in Section 3.2 below, assuming a pure Ar gas phase is a reasonable approximation. Then, if we use the material laws (2.2b) and (2.3a), the energy balance in the gas phase (2.1c) simplifies to

$$\frac{z^{(\text{Ar})} R}{M^{(\text{Ar})}} \frac{\partial}{\partial t} (\rho_{\text{gas}} T_{\text{gas}}) + \operatorname{div} \left(\frac{(z^{(\text{Ar})} + 1) R}{M^{(\text{Ar})}} \rho_{\text{gas}} T_{\text{gas}} \mathbf{v}_{\text{gas}} + \mathbf{q}_{\text{gas}} \right) = \rho_{\text{gas}} \mathbf{g} \bullet \mathbf{v}_{\text{gas}}, \tag{2.5}$$

and the heat flux satisfies Fourier's law, i.e.

$$\mathbf{q}_{\text{gas}} = -(\kappa^{(\text{Ar})} \nabla T_{\text{gas}}). \tag{2.6}$$

2.2 *SiC growth and sublimation, free boundaries*

Due to phase transitions and chemical reactions, all surfaces ambient to the growth chamber constitute free boundaries. The occurring processes include the intended growth of the single crystal and the sublimation of the source powder as well as unwanted processes such as graphitization of seed and source or the decomposition of the graphite walls.

A natural numerical approach is to calculate the position of the free boundaries at $t = t_1 = t_0 + \delta$, for a small positive δ, from its position at $t = t_0$. To proceed in this way, one needs to determine the species mass flux at each point of the free boundary from the values of the fields (2.4) at $t = t_0$.

In a first, crude, approximation, instead of taking into account the gas constituents Si, Si_2C, and SiC_2, one can consider a homogeneous "SiC-gas", determining the partial pressure $p^{(\text{SiC-gas})}$ of the SiC-gas from a diffusion equation. Assuming that, at the boundary of the gas phase (crystal surface, powder surface, or graphite wall, respectively), $p^{(\text{SiC-gas})}$ is identical to the corresponding temperature- and surface-dependent equilibrium pressure p^{eq} ($p^{\text{eq}} = p^{\text{eq}}_{\text{crystal}}$, $p^{\text{eq}}_{\text{powder}}$, or $p^{\text{eq}}_{\text{wall}}$, respectively) yields Dirichlet boundary conditions for the diffusion problem for $p^{(\text{SiC-gas})}$. The mass flux j between gas and surface can then be computed from the solution $p^{(\text{SiC-gas})}$. However, this approach supposes that the growth process is limited by the transport through the gas phase and it omits the influence of the growth kinetics.

To take into account the influence of the growth kinetics, one can use a Hertz–Knudsen formula to determine the mass flux j:

$$j = \frac{s\sqrt{M^{(\text{SiC})}}}{\sqrt{2\pi RT}}(p^{(\text{SiC-gas})} - p^{\text{eq}}), \tag{2.7}$$

which means replacing the Dirichlet conditions of the diffusion problem for $p^{(\text{SiC-gas})}$ with a Robin condition. In (2.7), $s \in [0, 1]$ is a surface-dependent sticking coefficient, denoting the probability for a molecule that collides with the surface to stick to that surface and be absorbed. At the graphite wall and at the powder surface, the value of s must also take into account that the surface is jagged and porous.

The above model of simple sublimation cannot describe and predict chemical effects such as the observed graphitization of the powder source. In order to include such effects, one has to consider several chemical reactions occurring at the surfaces, and one has to take into account at least the most important constituents of the SiC-gas, i.e. Si, Si_2C, and SiC_2. Then, instead of equilibrium pressures for the different components, one merely has relations between the different partial pressures in the equilibrium, resulting from the mass action laws of the chemical reactions considered. For example, from the reactions

$$2\text{SiC} \to \text{Si} + \text{SiC}_2, \qquad \text{SiC} + \text{Si} \to \text{Si}_2\text{C},$$

involving solid SiC and the main gas species, the mass action laws imply that there are temperature-dependent functions K_{I} and K_{II} such that, for the partial pressures of a gas mixture in equilibrium with the SiC crystal, we have

$$p^{(\text{Si})} p^{(\text{SiC}_2)} = K_{\text{I}}(T), \qquad \frac{p^{(\text{Si}_2\text{C})}}{p^{(\text{Si})}} = K_{\text{II}}(T). \tag{2.8}$$

Then (2.8) must be used to determine suitable boundary conditions for the reaction-diffusion equations (2.1d) above. Further research is ongoing to formulate such boundary conditions as well as the mass action laws for reactions changing the composition of the surface, to model the kinetics of the chemical reactions, and to determine the material parameters involved.

2.3 *Heat conduction in solid materials*

The PVT growth system comprises several solid material components (see Fig. 1).

Heat transport inside solid materials via conduction is considered in the current section. Radiative heat transfer through the semi-transparent seed crystal is included using the band model (see Section 2.5 below). Radiative heat transfer due to radiation which is both emitted and absorbed inside the same solid material β is included in the current model by using an appropriate temperature-dependent law for the thermal conductivity of the material β. However, the current model neglects any mechanical or chemical interactions inside the solid materials. In particular, it does not account for certain effects observed in real growth systems such as porosity changes, sintering and graphitization of the source powder, and accumulation of Si in the graphite felt insulation.

Heat conduction in the solid material β obeys

$$\rho^{[\beta]} c_{\mathrm{sp}}^{[\beta]} \frac{\partial T^{[\beta]}}{\partial t} + \operatorname{div} \mathbf{q}^{[\beta]} = f^{[\beta]}, \tag{2.9a}$$

$$\mathbf{q}^{[\beta]} = -\kappa^{[\beta]} \nabla T^{[\beta]}, \tag{2.9b}$$

where $T^{[\beta]}$ denotes absolute temperature, $\rho^{[\beta]}$ mass density, $c_{\mathrm{sp}}^{[\beta]}$ specific heat, $\mathbf{q}^{[\beta]}$ heat flux, $\kappa^{[\beta]}$ thermal conductivity, and $f^{[\beta]}$ power density (per volume) caused in conducting materials β due to induction heating. The heat sources $f^{[\beta]}$ are determined according to the sinusoidal RF-heating model in Section 2.6.

Heat conduction in the copper induction coil is not considered, as, in real growth systems, the coil is cooled very effectively, e.g., by water flowing inside the coil rings. Thereby, the coil is kept virtually at room temperature.

2.4 *Interface, boundary, and initial conditions*

To complete the heat transport model inside the entire growth apparatus, the heat equation of the gas phase (2.1c) and the different heat equations (2.9) for the solid materials β need to be coupled by appropriate interface conditions, and suitable outer boundary conditions have to be set. We assume that the locations of all solid components of the growth apparatus do not change with time.

Let β and β' denote different solid components of the growth apparatus. The normal heat flux is assumed to be continuous on an interface $\gamma_{\beta,\beta'}$ between two solid materials β and β', i.e. the interface condition is given by (2.10a). If the solid material β is semi-transparent, or on an interface $\gamma_{\beta',\mathrm{gas}}$ between the solid material β' and the gas phase, one needs to account for radiosity R and for irradiation J, resulting in interface conditions (2.10b) and (2.10c), respectively. The modeling of R and J is the subject of Section 2.5 below.

$$\mathbf{q}^{[\beta]} \bullet \mathbf{n}^{[\beta]} = \mathbf{q}^{[\beta']} \bullet \mathbf{n}^{[\beta]} \quad \text{on } \gamma_{\beta,\beta'}, \tag{2.10a}$$

$$\mathbf{q}^{[\beta]} \bullet \mathbf{n}^{[\beta]} - R + J = \mathbf{q}^{[\beta']} \bullet \mathbf{n}^{[\beta]} \quad \text{on } \gamma_{\beta,\beta'}, \tag{2.10b}$$

$$\mathbf{q}_{\text{gas}} \bullet \mathbf{n}_{\text{gas}} - R + J = \mathbf{q}^{[\beta]} \bullet \mathbf{n}_{\text{gas}} \quad \text{on } \gamma_{\beta,\text{gas}}, \tag{2.10c}$$

where $\mathbf{n}^{[\beta]}$ is the outer unit normal vector to the solid material β, and $\mathbf{n}_{\text{gas}}$ is the outer unit normal vector to the gas phase.

The temperature is always assumed to be continuous between solid materials, i.e., on an interface $\gamma_{\beta,\beta'}$ between two solid materials β and β', one has (2.11a). Even though, in reality, the temperature is also continuous across an interface $\gamma_{\beta,\text{gas}}$ between a solid material β and the gas phase as stated in (2.11b), the temperature gradient can be extremely steep inside an interface layer. If the size of the interface layer is much less than typical lengths of the system to be modeled, then it is reasonable to assume a temperature jump on the interface. In this case, if the heat flux in the gas phase satisfies Fourier's law (2.6), then the temperature discontinuity depends linearly on the normal heat flux through the interface, with a positive factor of proportionality ξ_β. Thus, (2.11b) is then replaced by (2.11b′).

$$T^{[\beta]} = T^{[\beta']} \quad \text{on } \gamma_{\beta,\beta'}, \tag{2.11a}$$

$$T^{[\beta]} = T_{\text{gas}} \quad \text{on } \gamma_{\beta,\text{gas}}, \tag{2.11b}$$

$$-(\kappa_{\text{gas}} \nabla T_{\text{gas}}) \bullet \mathbf{n}_{\text{gas}} = \xi_\beta (T_{\text{gas}} - T^{[\beta]}) \quad \text{on } \gamma_{\beta,\text{gas}}. \tag{2.11b′}$$

The Stefan–Boltzmann law together with (2.9b) provides the outer boundary condition

$$-(\kappa^{[\beta]} \nabla T^{[\beta]}) \bullet \mathbf{n}^{[\beta]} = \sigma \epsilon^{[\beta]} ((T^{[\beta]})^4 - T_{\text{room}}^4), \tag{2.12}$$

where $\sigma = 5.6696 \cdot 10^{-8} \text{W/m}^2\text{K}^4$ denotes the Boltzmann radiation constant, and $\epsilon^{[\beta]}$ denotes the (temperature-dependent) emissivity of the surface. Condition (2.12) means that the growth apparatus is exposed to a black body environment (e.g. a large isothermal room) radiating at room temperature $T_{\text{room}} = 293$ K.

On outer boundaries receiving radiation from other parts of the apparatus, the situation is more complicated. On such boundaries, it does not suffice to use just the Stefan–Boltzmann law according to (2.12), but, as in (2.10b) and (2.10c), one has to account for radiosity R and irradiation J, leading to the boundary condition

$$\mathbf{q}^{[\beta]} \bullet \mathbf{n}^{[\beta]} - R + J = 0, \tag{2.13}$$

where, as before, the modeling of R and J is deferred to Section 2.5.

Condition (2.13) is used on outer boundaries representing surfaces adjacent to the upper and lower blind hole in Fig. 1. To allow for radiative interactions between such open cavities and the ambient environment, including reflections at the cavity's surfaces, black body phantom closures are used, emitting radiation at T_{room}. In Fig. 1, the phantom closures are the dashed lines labeled Γ_{top} and Γ_{bottom}.

Finally, in the case of transient simulations, one needs to prescribe a temperature distribution at the initial time. For the simulations presented in Section 3.2, it is assumed that the initial temperature distribution is homogeneous at T_{room}.

2.5 *Diffuse-gray radiation*

The heat flux due to radiosity R and the heat flux due to irradiation J had to be included in the interface conditions between a solid and a semi-transparent material and between a solid material

and the gas phase, resulting in the above interface conditions (2.10b) and (2.10c), respectively. Similarly, the heat fluxes due to R and J have to be taken into account on outer boundaries being in mutual radiative interaction. The resulting outer boundary condition was stated as (2.13). The subject of the present section is the modeling of R and J.

The model does not consider any interaction between gas and radiation. In particular, radiation is assumed to travel unperturbed between surfaces of solid components throughout cavities inside the growth apparatus. All solids except the SiC single crystal are treated as opaque media. For the SiC single crystal, semi-transparency is included via the band approximation model.

Reflection and emittance are supposed to be diffuse-gray, i.e. independent of the angle of incidence and independent of the wavelength. Since the solid surfaces inside the growth apparatus (including the surface of the SiC single crystal) are generally non-smooth, the effect of specular reflections is expected to be negligible.

The model employs the net radiation method as described in [8, Chapter 3.3] and, with a different notation, in [5]. More general treatments of this standard model can be found in textbooks such as [14] and [23]. We are first going to describe the opaque case, and, subsequently, we will indicate modifications in the case of semi-transparency.

In the opaque case, no radiation is transmitted through a solid surface Γ, and at each point $\mathbf{x} \in \Gamma$, the radiosity R is the sum of the contribution from emitted radiation E and of the contribution from reflected radiation J_{ref}:

$$R(\mathbf{x}) = E(\mathbf{x}) + J_{\text{ref}}(\mathbf{x}). \tag{2.14}$$

It is convenient to write the material dependence of the emissivity as a dependence on the space variable $\mathbf{x}$: $\epsilon(T_{\text{solid}}(\mathbf{x}), \mathbf{x}) := \epsilon^{[\beta]}(T_{\text{solid}}(\mathbf{x}))$ for each $\mathbf{x}$ in the domain of the solid β, where T_{solid} denotes the absolute temperature in the solid material adjacent to the cavity considered. While, due to the possible temperature jump between solid and gas (cf. (2.11b′)), one needs to distinguish between the corresponding temperatures, such a distinction is not necessary between the temperatures in different solids, as continuity is assumed on solid-solid interfaces.

According to the Stefan–Boltzmann law, the emitted radiation is given by

$$E(\mathbf{x}) = \sigma \cdot \epsilon(T_{\text{solid}}(\mathbf{x}), \mathbf{x}) \cdot (T_{\text{solid}}(\mathbf{x}))^4. \tag{2.15}$$

The reflective term in (2.14) can be expressed using the reflectivity ϱ, i.e. the ratio of reflected radiation and irradiation J:

$$J_{\text{ref}}(\mathbf{x}) = \varrho(T_{\text{solid}}(\mathbf{x}), \mathbf{x}) \cdot J. \tag{2.16}$$

If α denotes the absorptivity, i.e. the ratio of absorbed radiation and irradiation, then opaqueness implies

$$\alpha + \varrho = 1, \tag{2.17}$$

and by Kirchhoff's law

$$\alpha = \epsilon. \tag{2.18}$$

Due to diffuseness, J can be calculated using the integral operator $\mathcal{J}$ defined by

$$J(\mathbf{x}) = \mathcal{J}(R)(\mathbf{x}) := \int_\Gamma \Lambda(\mathbf{x}, \mathbf{y}) \omega(\mathbf{x}, \mathbf{y}) R(\mathbf{y}) \, \mathrm{d}\mathbf{y}, \tag{2.19}$$

where Λ is the visibility factor defined by

$$\Lambda(\mathbf{x}, \mathbf{y}) := \begin{cases} 1 & \text{if } \mathbf{x}, \mathbf{y} \text{ are mutually visible,} \\ 0 & \text{if } \mathbf{x}, \mathbf{y} \text{ are mutually invisible,} \end{cases} \tag{2.20}$$

and where ω is the view factor, for $\mathbf{x} \neq \mathbf{y}$, defined by

$$\omega(\mathbf{x}, \mathbf{y}) := \frac{(\mathbf{n}_{\text{gas}}(\mathbf{y}) \bullet (\mathbf{x} - \mathbf{y}))(\mathbf{n}_{\text{gas}}(\mathbf{x}) \bullet (\mathbf{y} - \mathbf{x}))}{\pi((\mathbf{y} - \mathbf{x}) \bullet (\mathbf{y} - \mathbf{x}))^2}. \tag{2.21}$$

Combining Equations (2.14) through (2.19) provides the following nonlocal equation for the radiosity R:

$$R(\mathbf{x}) - (1 - \epsilon(T_{\text{solid}}(\mathbf{x}), \mathbf{x}))\mathcal{J}(R)(\mathbf{x}) = \sigma \cdot \epsilon(T_{\text{solid}}(\mathbf{x}), \mathbf{x}) \cdot (T_{\text{solid}}(\mathbf{x}))^4. \tag{2.22}$$

Finally, as it is needed in the interface conditions (2.10b) and (2.10c), and in the outer boundary condition (2.13), the expression $-R + J$ is computed from (2.22) and (2.19):

$$-R(\mathbf{x}) + J(\mathbf{x}) = \epsilon(T_{\text{solid}}(\mathbf{x}), \mathbf{x}) \cdot (\mathcal{J}(R)(\mathbf{x}) - \sigma(T_{\text{solid}}(\mathbf{x}))^4). \tag{2.23}$$

The new formulation of (2.10b) and (2.10c) will be given after the discussion of the semi-transparent case below (see (2.28)). However, the open cavities of the apparatus are typically not adjacent to the seed crystal (see Fig. 1). This allows one to rewrite the outer boundary condition (2.13) as

$$\mathbf{q}^{[\beta]} \bullet \mathbf{n}^{[\beta]} + \epsilon \cdot (\mathcal{J}(R) - \sigma T_{\text{solid}}^4) = 0 \tag{2.24}$$

on each outer boundary of solid material β adjacent to an open radiation region.

In the following, we describe the band approximation model to account for the semi-transparency of the SiC single crystal.

According to the band approximation model, the spectrum decomposes into a *reflective* band of wavelengths I_{r} and a *transmittive* band of wavelengths I_{t}. Radiation corresponding to I_{r} interacts with the surface of the semi-transparent material, i.e. it is emitted, reflected and absorbed by the surface. Radiation corresponding to I_{t} does not interact with the semi-transparent material at all, i.e. it is transmitted unperturbed through the medium. Thus, the band model neglects radiation transmitted between the interior and the exterior of the semi-transparent material. This is an accurate approximation if the range of wavelengths in which the spectral optical thickness (penetration depth divided by material thickness) is close to one, is sufficiently small [5, Section 3.4]. As mentioned before, radiation-driven heat transport staying inside a solid component is assumed to be accounted for by the corresponding temperature-dependent law of thermal conductivity.

The contributions from the two bands of wavelengths are computed separately. While the radiation region for the reflective band consists of the actual cavity, the radiation region for the transmittive band is made up of the cavity united with the semi-transparent body. Consequently, the boundary Γ_{t} of the transmittive radiation region is different from the boundary Γ of the opaque case, Γ_{t} containing the interfaces between semi-transparent material and opaque solids instead of interfaces between semi-transparent body and gas.

On Γ, let R_{r}, E_{r}, and $J_{\text{ref,r}}$ denote the respective contributions to the radiosity, emitted radiation, and reflected radiation stemming from wavelengths in the reflective band I_{r}. These quantities satisfy (2.14), whereas Planck's law of black body radiation implies that, for E_{r}, the emissivity ϵ written in (2.15) has to be replaced by

$$\epsilon_{\text{r}}(T_{\text{solid}}(\mathbf{x}), \mathbf{x}) = \int_{I_{\text{r}}} \epsilon(T_{\text{solid}}(\mathbf{x}), \mathbf{x}, \lambda)\, I_{\text{b},\lambda}(T_{\text{solid}}(\mathbf{x}))\, \mathrm{d}\lambda\,, \tag{2.25}$$

$$I_{\text{b},\lambda}(T) := \frac{15C^4}{\pi^4 \lambda^5 T^4 (e^{C/\lambda T} - 1)}, \tag{2.26}$$

λ denoting the wavelength, $\epsilon(T_{\text{solid}}(\mathbf{x}), \mathbf{x}, \lambda)$ denoting the emissivity for monochromatic radiation of wavelength λ, and $C := 1.4388 \cdot 10^{-2}$ mK.

Moreover, using Planck's and Kirchhoff's laws to determine the absorptivity of Γ with respect to the reflective band, one can show that (2.16) also holds for R_{r} and $J_{\text{ref,r}}$ if $\varrho(\mathbf{x}, T(\mathbf{x}))$ is replaced by

$$\varrho_{\text{r}}(T_{\text{solid}}(\mathbf{x}), \mathbf{x}) = 1 - \frac{\epsilon_{\text{r}}(T_{\text{solid}}(\mathbf{x}), \mathbf{x})}{\int_{I_{\text{r}}} I_{\text{b},\lambda}(T_{\text{solid}}(\mathbf{x}))\, \mathrm{d}\lambda}. \tag{2.27}$$

As in the opaque case, one can now derive a nonlocal equation for R_{r}, similar to (2.22).

Let R_{t}, E_{t}, $J_{\text{ref,t}}$, ϵ_{t}, and ϱ_{t} denote the quantities with respect to the transmittive band, corresponding to R_{r}, E_{r}, $J_{\text{ref,r}}$, ϵ_{r}, and ϱ_{r}, respectively. The procedure to compute the transmittive contributions is analogous to the reflective case, with Γ_{t} used instead of Γ. By $\mathcal{J}_{\text{t}}$, we denote the operator corresponding to $\mathcal{J}$ with Γ replaced by Γ_{t}; ϵ_{t} and ϱ_{t} are computed by replacing I_{r} with I_{t} in both (2.25) and (2.27).

One is now in a position to rewrite (2.10b) and (2.10c) depending on which of the following three cases occurs at the respective interface:

Case (i): The interface is part of $\Gamma_{\text{t}} \setminus \Gamma$, i.e. it is an interface between the semi-transparent SiC single crystal and an opaque solid β. Let the interface be denoted by $\gamma_{\text{SiC-Crystal},\beta}$. Since only transmittive contributions are present on $\gamma_{\text{SiC-Crystal},\beta}$, the interface condition reads

$$\mathbf{q}^{[\text{SiC-Crystal}]} \bullet \mathbf{n}^{[\text{SiC-Crystal}]} + \epsilon_{\text{t}} \cdot (\mathcal{J}_{\text{t}}(R_{\text{t}}) - \sigma T_{\text{solid}}^4) = \mathbf{q}^{[\beta]} \bullet \mathbf{n}^{[\text{SiC-Crystal}]} \quad \text{on } \gamma_{\text{SiC-Crystal},\beta}. \tag{2.28a}$$

Case (ii): The interface is part of $\Gamma_{\text{t}} \cap \Gamma$, i.e. it lies between an opaque solid β and the gas phase. Let the interface be called $\gamma_{\beta,\text{gas}}$. On $\gamma_{\beta,\text{gas}}$, one obtains contributions from both bands I_{r} and I_{t}, which are then incorporated additively into the corresponding interface condition, yielding

$$\mathbf{q}_{\text{gas}} \bullet \mathbf{n}_{\text{gas}} + \epsilon_{\text{r}} \cdot (\mathcal{J}_{\text{r}}(R_{\text{r}}) - \sigma T_{\text{solid}}^4) + \epsilon_{\text{t}} \cdot (\mathcal{J}_{\text{t}}(R_{\text{t}}) - \sigma T_{\text{solid}}^4) = \mathbf{q}^{[\beta]} \bullet \mathbf{n}_{\text{gas}} \quad \text{on } \gamma_{\beta,\text{gas}}. \tag{2.28b}$$

Case (iii): The interface is part of $\Gamma \setminus \Gamma_{\text{t}}$, i.e. the interface is between the SiC crystal and the gas phase. Hence, it will be denoted by $\gamma_{\text{SiC-Crystal,gas}}$. On $\gamma_{\text{SiC-Crystal,gas}}$, only contributions from the reflective band are present, resulting in

$$\mathbf{q}_{\text{gas}} \bullet \mathbf{n}_{\text{gas}} + \epsilon_{\text{r}} \cdot (\mathcal{J}_{\text{r}}(R_{\text{r}}) - \sigma T_{\text{solid}}^4) = \mathbf{q}^{[\text{SiC-Crystal}]} \bullet \mathbf{n}_{\text{gas}} \quad \text{on } \gamma_{\text{SiC-Crystal,gas}}. \tag{2.28c}$$

2.6 *Induction heating*

The goal of the present section is to determine the heat sources $f^{[\beta]}$ occurring in (2.9a), that are due to the radio frequency (RF) induction heating of the PVT growth system. The model presented in the following assumes an axisymmetric growth apparatus and takes its basic ideas from [4] and [18].

To be able to consider the problem in an axisymmetric setting, the actual coil is replaced by N cylindrical rings with a sinusoidal alternating voltage imposed in each ring. Thus, the voltage imposed in the k-th ring has the complex representation

$$v_k(t) = v_{k,0} e^{i\omega t}, \tag{2.29}$$

where i denotes the imaginary unit, ω is the angular frequency, and $v_{1,0}, \ldots, v_{N,0}$ are complex-valued voltages. Let (r, ϑ, z) denote cylindrical coordinates. It is shown in [4] and [18] that, given

the total voltage in each coil ring $v_{k,0}$, $k = 1, \ldots, N$, there is a complex-valued magnetic scalar potential ϕ such that the following holds for the current density $\mathbf{j}$ (cf. [18, Eq. (28)]): $\mathbf{j} = j_0 e^{i\omega t}\mathbf{e}_\vartheta$, with

$$j_0 = \begin{cases} -i\omega\sigma_c\phi + \frac{\sigma_c v_{k,0}}{2\pi r} & \text{in the } k\text{-th coil ring,} \\ -i\omega\sigma_c\phi & \text{in all other conducting materials,} \end{cases} \tag{2.30}$$

where σ_c denotes the electrical conductivity. The heat sources $f^{[\beta]} = f(r, z)$ can then be computed from

$$f(r, z) = \frac{|j_0(r, z)|^2}{2\sigma_c(r, z)}. \tag{2.31}$$

All solid materials in the growth system are considered as potential conductors, whereas the gas phase is treated as a perfect insulator. We assume that displacement currents as well as surface currents can be neglected.

The potential ϕ is determined from the system of elliptic partial differential equations [18, (22), (29)], which we rewrite in the following divergence form (2.32) which is more suitable for our numerical approach via a finite volume discretization:

$$-\nu \operatorname{div} \frac{\nabla(r\phi)}{r^2} = 0 \qquad \text{in the gas phase,} \tag{2.32a}$$

$$-\nu \operatorname{div} \frac{\nabla(r\phi)}{r^2} + \frac{i\omega\sigma_c\phi}{r} = \frac{\sigma_c v_{k,0}}{2\pi r^2} \qquad \text{in the } k\text{-th coil ring,} \tag{2.32b}$$

$$-\nu \operatorname{div} \frac{\nabla(r\phi)}{r^2} + \frac{i\omega\sigma_c\phi}{r} = 0 \qquad \text{in other conducting materials,} \tag{2.32c}$$

where ν denotes the magnetic reluctivity, i.e. the reciprocal of the magnetic permeability. Both ν and σ_c can vary in space, but they are supposed to be constant in time.

The system (2.32) is completed by interface and boundary conditions. Owing to the assumption of no surface currents, we have the interface conditions [18, (30)]:

$$\left(\frac{\nu\restriction_{\text{Material}_1}}{r^2} \nabla(r\phi)\restriction_{\text{Material}_1} \right) \bullet \mathbf{n}_{\text{Material}_1} = \left(\frac{\nu\restriction_{\text{Material}_2}}{r^2} \nabla(r\phi)\restriction_{\text{Material}_2} \right) \bullet \mathbf{n}_{\text{Material}_1} \tag{2.33}$$

on interfaces between Material_1 and Material_2, where $\restriction$ denotes the restriction to the respective material, and $\mathbf{n}_{\text{Material}_1}$ denotes the outer unit normal vector to Material_1. It is also assumed that ϕ is continuous throughout the whole domain and that $\phi = 0$ both on the symmetry axis $r = 0$ and sufficiently far from the growth apparatus. For the apparatus of radius 13.6 cm (including coil) and of height 25 cm used for the numerical simulations discussed in Section 3.2 below, we found from numerical experiments that using a domain radius and height of 1.2 m and 1.8 m, respectively, is sufficiently accurate for our purposes.

Let Ω_k denote the two-dimensional domain of the k-th coil ring. The total current in the k-th ring is then given by $e^{i\omega t} J_k$, with

$$J_k := \int_{\Omega_k} j_0(x)\, \mathrm{d}x\,. \tag{2.34}$$

Since the coil rings constitute the approximation of a single, connected coil, the total current must be the same in each coil ring, i.e.

$$J_k = J_{k+1} \quad \text{for } k = 1, \ldots, N-1. \tag{2.35}$$

One can now set up a linear system for $v_{1,0}, \dots, v_{N,0}$ such that (2.35) is satisfied, and one has the freedom to prescribe a total current or a total voltage or (as we do for our simulations in Section 3.2) a total power (see [10] for more details).

The assumption of a sinusoidal form of the eletromagnetic quantities is only admissible if the material parameters involved are constant in time, and if there is no movement. Thus, to account for the temperature dependence of the electrical conductivity during the transient simulations in Section 3.2, the quasi-stationary electromagnetic problem presented above is solved in each time step of the transient computations for the heat evolution problem.

3. Numerical solutions

3.1 *Finite volume scheme*

In the following Section 3.2, we will present results of numerical simulations for the temperature evolution in the growth system. Simplifying assumptions, as explained in Section 3.2.1, lead to a coupled system of equations of the form

$$\frac{\partial \varepsilon_j(T,x)}{\partial t} - \operatorname{div}(\kappa_j(T)\nabla T) - f_j(T,t,x) = 0 \tag{3.1}$$

for the unknown continuous temperature function T. Here, each equation (3.1) is considered on a time space cylinder $[0, t_f]\times\Omega_j$, where Ω_j is a two-dimensional polytope (a bounded polyhedral set), representing either a solid component of the growth apparatus or the gas phase. The goal is now to discretize the system and to state a discrete existence and uniqueness result that was proved in [16]. Here, for simplicity, we restrict ourselves to the continuous interface conditions for temperature and heat flux and to the outer boundary condition (2.12). For the general case, including discontinuous and nonlocal interface and boundary conditions as well as convective contributions, we refer to [16].

Time discretization is performed using the implicit Euler scheme, where $0 = t_0 < \cdots < t_N = t_f$, $N \in \mathbb{N}$. For subsequent use, let $k_n := t_n - t_{n-1}$, $\Delta := \max\{k_n : n = 1, \dots, N\}$. The space domain $\Omega := \bigcup_j \Omega_j$ is discretized into sufficiently benign control volumes, e.g., by the following procedure: Let Ω_c denote the convex hull of Ω, and consider a constrained Delaunay triangulation of Ω_c. Such a triangulation must satisfy the constrained Delaunay criterion, i.e. it must consist of triangles such that the sum of two angles opposite the same connecting edge can be at most 180°, and angles opposite boundaries or interfaces must be at most 90° (see Fig. 2).

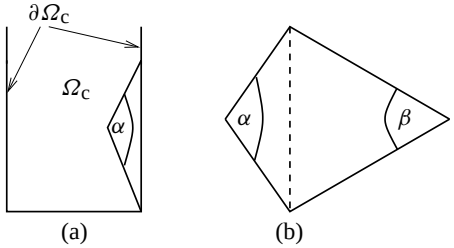

FIG. 2. The situation in (a) violates the constrained Delaunay criterion, as $\alpha > 90°$. For the situation in (b), $\alpha = 110°$ and $\beta = 60°$, i.e. the constrained Delaunay criterion is violated if and only if the dashed line constitutes not only a common edge of two triangles, but also an interface between different domains Ω_{j_1} and Ω_{j_2}.

Moreover, each interface must be discretized into triangle edges (see [22] for further information on two-dimensional Delaunay triangulation). If V denotes the (finite) set of vertices of the constraint Delaunay triangulation, then, for each $v \in V$,

$$\omega_v := \overline{\{x \in p : \|x - v\|_2 < \|x - w\|_2 \text{ for each } w \in V \setminus \{v\}\}} \tag{3.2}$$

is the Voronoï box centered at v. For each j and each $v \in V$, let $\omega_{j,v} := \omega_v \cap \Omega_j$. Now, for each j, $\Omega_j = \bigcup_{v \in V_j} \omega_{j,v}$, where $V_j := V \cap \Omega_j$, is the desired discretization of Ω_j into control volumes $\omega_{j,v}$. Finally, letting $V_\Omega := V \cap \Omega$, we are in a position to formulate the finite volume scheme for the unknown temperature: One is seeking a nonnegative solution $(\mathbf{T}_0, \ldots, \mathbf{T}_N)$, $\mathbf{T}_n = (T_{n,v})_{v \in V_\Omega}$, to

$$T_{0,v} = T_{\text{room}} \qquad (v \in V_\Omega), \tag{3.3a}$$

$$\mathcal{H}_{n,v}(\mathbf{T}_{n-1}, \mathbf{T}_n) = 0 \qquad (v \in V_\Omega,\ n \in \{1, \ldots, N\}), \tag{3.3b}$$

where for each $n \in \{1, \ldots, N\}$:

$$\begin{aligned}
&\mathcal{H}_{n,v}(\mathbf{T}_{n-1}, \mathbf{T}_n) \\
&\quad := k_n^{-1} \sum_j (\varepsilon_j(T_{n,v}, v) - \varepsilon_j(T_{n-1,v}, v)) \cdot v_r \cdot \lambda_2(\omega_{j,v}) \\
&\qquad - \sum_j \sum_{w \in \mathrm{nb}_j(v)} \frac{\kappa_j(T_{n,v}) \cdot v_r + \kappa_j(T_{n,w}) \cdot w_r}{2} \cdot \frac{T_{n,w} - T_{n,v}}{\|v - w\|_2} \cdot \lambda_1(\omega_{j,v} \cap \omega_{j,w}) \\
&\qquad + \sum_j \sigma \epsilon_j(T_{n,v}) \cdot (T_{n,v}^4 - T_{\text{room}}^4) \cdot v_r \cdot \lambda_1(\partial\omega_{j,v} \cap \partial\Omega) \\
&\qquad - \sum_j f_j(T_{n,v}, t_n, v) \cdot v_r \cdot \lambda_2(\omega_{j,v}).
\end{aligned} \tag{3.4}$$

In (3.4), λ_2 and λ_1 denote 2-dimensional and 1-dimensional Lebesgue measure, respectively, and $\mathrm{nb}_j(v) := \{w \in V_j \setminus \{v\} : \lambda_1(\omega_{j,v} \cap \omega_{j,w}) \neq 0\}$ is the set of j-neighbors of v. Note that the occurrence of v_r and w_r in (3.4) is due to the use of cylindrical coordinates, where $v = (v_r, v_z)$, $w = (w_r, w_z)$.

THEOREM 1 Assume (i)–(iv):

(i) $\varepsilon_j \geqslant 0$, $\kappa_j \geqslant 0$, $\epsilon_j \geqslant 0$, and $f(0, t, x) \geqslant 0$.
(ii) $\varepsilon_j(\cdot, x)$ is increasing, and there is $L > 0$ such that $|\varepsilon_j(T, x) - \varepsilon_j(\tilde{T}, x)| \geqslant L\,|T - \tilde{T}|$ for each $x \in \Omega_j$.
(iii) κ_j, ϵ_j, and f_j are locally Lipschitz in T.
(iv) f_j is bounded from above.

Then there is $M > 0$ (independent of the time discretization) and Δ_M such that, for $\Delta < \Delta_M$, the finite volume scheme (3.3) has a unique solution $(\mathbf{T}_0, \ldots, \mathbf{T}_N) \in ([0, M]^{V_\Omega})^{N+1}$.

Proof. See [16, Theorem 3.8.35], where Theorem 1 has been proved in a more general context. □

3.2 *Numerical experiments*

3.2.1 *General setting.* In Sections 3.2.2 and 3.2.3 below, we present results of numerical simulations that give insight into transient temperature phenomena relevant to the PVT growth process. All numerical simulations presented in the following were performed for the growth system [17, Fig. 2] displayed in Fig. 1, consisting of an axisymmetric container having a radius of 8.4 cm and a height of 25 cm placed inside of 5 hollow rectangular-shaped copper induction rings. The geometric proportions of the coil rings are provided in Fig. 3. It is assumed that all relevant physical quantities are axisymmetric.

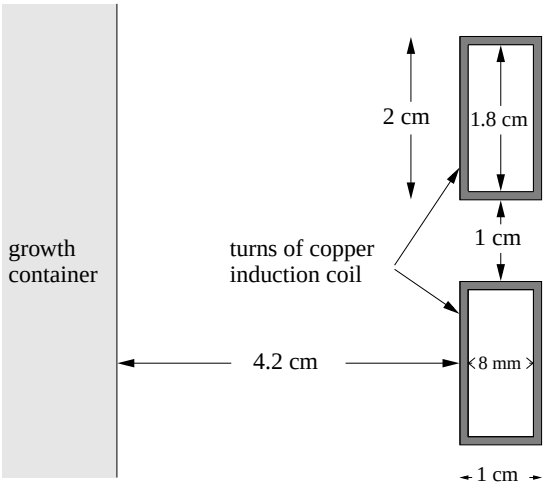

FIG. 3. Geometric proportions of induction coil rings.

All simulations presented in this article were performed for an idealized growth apparatus, treating all solid materials as homogeneous and pure. The material data used for the following numerical experiments are precisely the data provided in the appendices of [11] and [12], respectively.

Furthermore, it is assumed that the gas phase is made up solely of argon, which is a reasonable assumption for simulations of the temperature distribution evolution, as was described at the end of Section 2.1. Since we are neglecting convective contributions inside the gas phase for simplicity (see [12] for numerical simulations including convection), the energy balance in the gas phase is (2.5) with $\mathbf{v}_{\text{gas}} = 0$.

In absence of data on transition coefficients ξ_β (cf. (2.11b′)), for the presented simulations, the temperature is assumed to be continuous throughout the whole apparatus.

Discretization is performed using a finite volume scheme as described in Section 3.1 above, where additional terms arise from the nonlocal radiation operators. The resulting nonlinear discrete systems are solved by Newton's method.

The finite volume discretization of the nonlocal radiation terms according to Section 2.5 involves the calculation of visibility and view factors according to (2.19) – (2.21). Even for an axisymmetric configuration, in general, this is a complicated task. The method used is based on [5] and is described in [12, Sec. 4].

The angular frequency used for the induction heating is $\omega = 2\pi f$, where $f = 10$ kHz. The average total power P is prescribed according to the following linear ramp:

$$P(t) := \begin{cases} \frac{P_{\max}}{t_{\text{ramp}}} \cdot t & \text{for } 0 \leqslant t \leqslant t_{\text{ramp}}, \\ P_{\max} & \text{for } t \geqslant t_{\text{ramp}}, \end{cases} \tag{3.5}$$

where $t_{\text{ramp}} = 2$ h. Moreover, $P_{\max} = 7$ kW, except for the experiments depicted in Fig. 5. The distribution of the heat sources is redetermined in each time step of the transient problem for the temperature evolution to account for the time-dependent prescribed power as well as for the temperature dependence of the electrical conductivity.

Each simulation starts at $T_{\text{room}} = 293$ K, computing and monitoring the evolution of the temperature distribution in the growth apparatus.

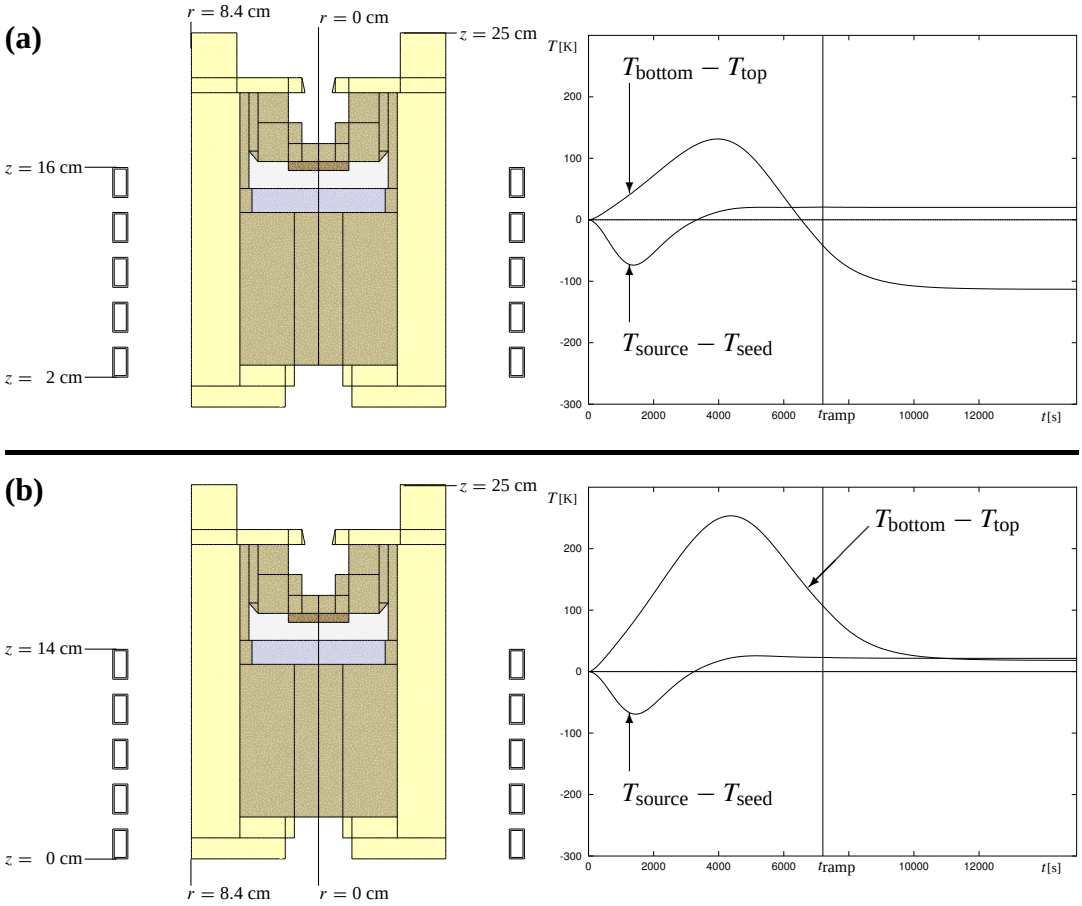

FIG. 4. The evolution of the temperature differences $T_{\text{bottom}} - T_{\text{top}}$ and $T_{\text{source}} - T_{\text{seed}}$ is compared for two different positions of the induction coil. The respective positions of the induction coil are given by the specifications on the left-hand side. For the locations of T_{bottom}, T_{top}, T_{source}, and T_{seed}, we refer to Fig. 1. The heating power is increased linearly according to (3.5) with $P_{\max} = 7$ kW.

All simulations were performed using the **WIAS Hi**gh **T**emperature **N**umerical **I**nduction **H**eating **S**imulator (**WIAS-HiTNIHS**), which is a software based on the program package *pdelib* being developed at the Weierstrass Institute of Applied Analysis and Stochastics (WIAS), Berlin [6].

3.2.2 *Temperature differences.* In a series of four numerical experiments, we investigate the relation between the temperature differences $T_{\rm bt} := T_{\rm bottom} - T_{\rm top}$ and $T_{\rm ss} := T_{\rm source} - T_{\rm seed}$ (cf. Fig. 1): We consider two different positions for the induction coil, and, for the lower coil position, three different values of $P_{\rm max}$ (cf. (3.5)). The relation between $T_{\rm bt}$ and $T_{\rm ss}$ is of importance, as in physical growth experiments, $T_{\rm bottom}$ and $T_{\rm top}$ are measured, and $T_{\rm bt}$ is often used as an indicator for $T_{\rm ss}$ which is not accessible to direct measurements, but crucial for the growth process.

For the two simulations using $P_{\rm max} = 7$ kW, the results for the respective evolutions of $T_{\rm bt}$ and $T_{\rm ss}$ are depicted in Fig. 4. In Fig. 4(a), the coil is in the higher position, between vertical coordinates $z = 2$ cm and $z = 16$ cm, and in Fig. 4(b), the coil is in the lower position, between $z = 0$ cm and $z = 14$ cm.

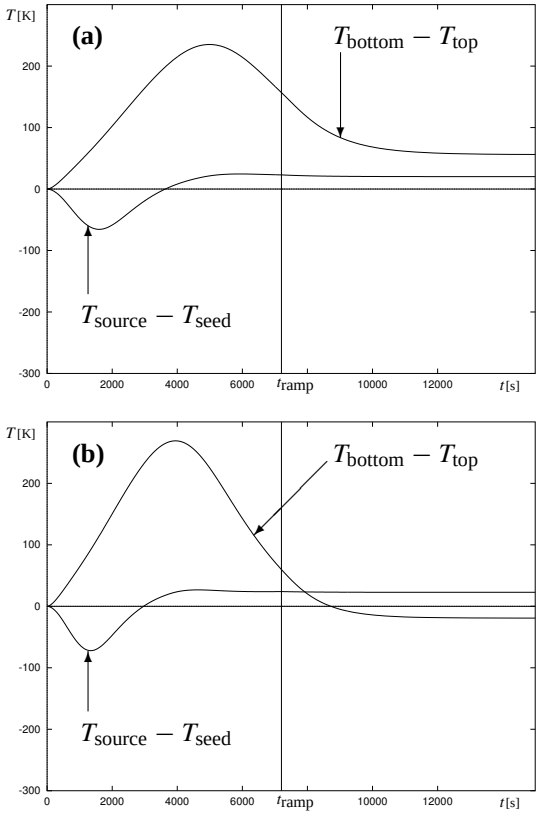

FIG. 5. As in Fig. 4(b), the evolution of the temperature differences $T_{\rm bottom} - T_{\rm top}$ and $T_{\rm source} - T_{\rm seed}$ is depicted for numerical experiments using the lower coil position. In contrast to Fig. 4(b), the power $P_{\rm max}$ in (3.5) is set to 5.5 kW in Fig. 5(a) and to 8.5 kW in Fig. 5(b).

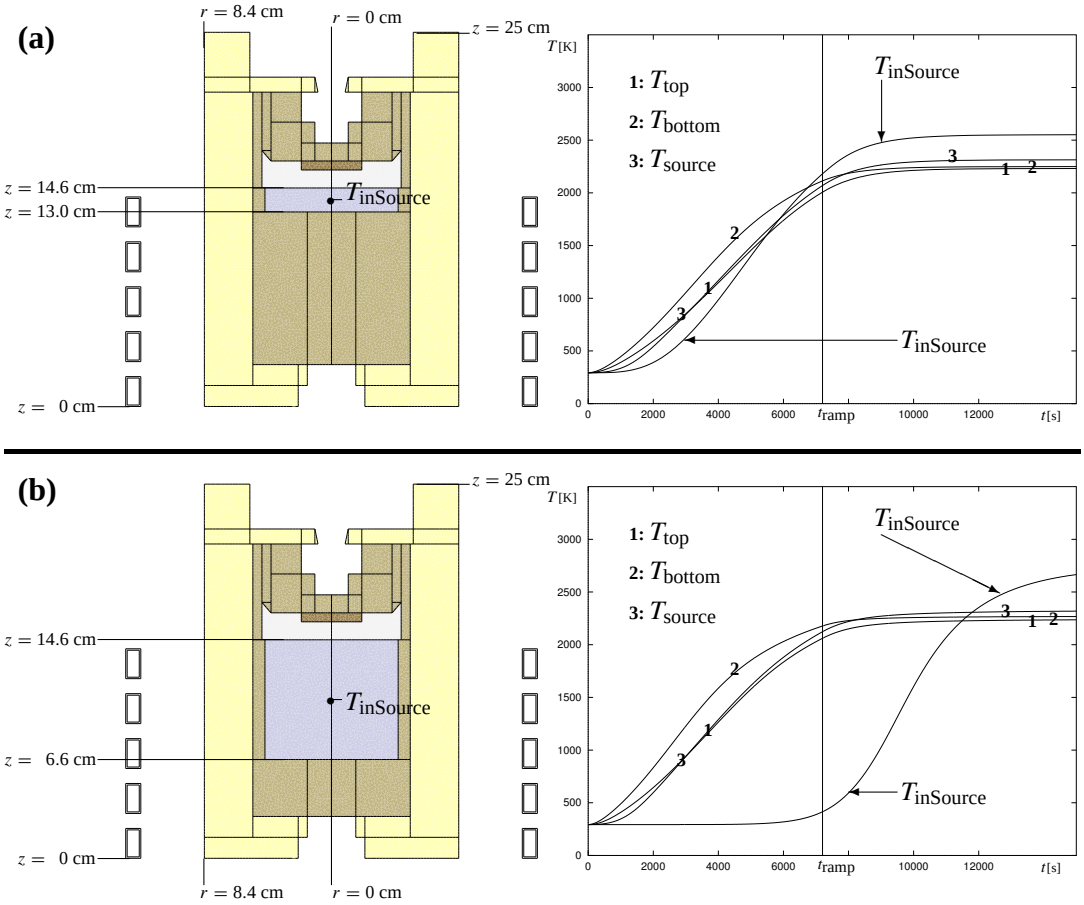

FIG. 6. The evolution of T_{inSource} is compared to the evolutions of T_{top}, T_{bottom}, and T_{source} for two different amounts of the powder charge. In comparison with (a), the amount of the powder is 5-fold in (b). For the locations of T_{top}, T_{bottom}, and T_{source}, see Fig. 1. The heating power is increased linearly according to (3.5) with $P_{\max} = 7$ kW.

TABLE 1

Time lag between T_{top} reaching 1200 K and T_{inSource} reaching 1200 K for the numerical experiments considered in Fig. 6

	$t_1 := t(T_{\text{top}} = 1200\text{ K})$ [min]	$t_2 := t(T_{\text{inSource}} = 1200\text{ K})$ [min]	$t_2 - t_1$ [min]
Fig. 6(a)	70	75	5
Fig. 6(b)	63	155	92

Figure 4 shows that the evolution of T_{ss} is almost identical for the two coil positions, whereas the behavior of T_{bt} changes drastically. In both cases, T_{bt} is no indicator for T_{ss} before T_{ss} has reached its quasi-stationary final state, but, more importantly, even in the stationary state at growth temperature, T_{ss} and T_{bt} are of comparable magnitude only for the lower coil position. In Fig. 4(a), not even the signs of T_{ss} and T_{bt} agree in the final state.

Moreover, the good agreement of T_{ss} and T_{bt} in the final state of Fig. 4(b) is merely coincidental in the sense that the agreement is lost for other values of P_{max}. For the same coil position as in Fig. 4(b), Fig. 5 shows that T_{bt} is almost three times as large as T_{ss} in the final state if P_{max} is reduced to 5.5 kW (Fig. 5(a)), and that T_{bt} and T_{ss} have different signs if P_{max} is increased to 8.5 kW (Fig. 5(b)).

The numerical experiments show that for the configuration considered, there is generally no easy relation between T_{ss} and T_{bt}. Even though there might be configurations where the situation is better, for each real growth system, the validity of using T_{bt} as an indicator for T_{ss} needs to be verified by some other method (e.g. numerical simulation).

3.2.3 *Heating of SiC source powder.* In two numerical experiments, we investigate the evolution of the temperature at the center of the SiC powder source in comparison with the temperature evolutions of T_{top}, T_{bottom}, and T_{source} (cf. Fig. 1). We consider two different quantities of the powder charge. In comparison with the experiment depicted in Fig. 6(a), the amount of SiC powder is fivefold in Fig. 6(b).

The low coil position of Fig. 4(b) was used for the simulations considered in the following. However, we note that we found similar results for the higher coil position used in Fig. 4(a).

Figure 6 shows that for the configuration considered, there is a time lag between the heating of the bulk of the apparatus and the heating of the interior of the SiC powder charge. While the evolution of T_{top}, T_{bottom}, and T_{source} is almost independent of the relevant powder quantities, the heating of the powder's center is significantly more delayed in Fig. 6(b).

As described in the Introduction, the growth system is usually kept at some 1200 K and at low pressure for a certain time, to bake out contaminants from the source powder. Table 1 shows that while the time lag between T_{top} reaching 1200 K and $T_{inSource}$ reaching 1200 K is merely 5 minutes for the smaller powder charge, it increases to 1.5 hours for the larger powder charge. Thus, depending on the configuration of the growth system, it can be of paramount importance to take into account this time lag, in order to allow sufficient time for the contaminant bake-out phase.

Acknowledgements

We thank Klaus Böttcher, Detlev Schulz, and Dietmar Siche of the Institute for Crystal Growth, Berlin, for helpful discussions and advice.

REFERENCES

1. BARRETT, D. L., MCHUGH, J. P., HOBGOOD, H. M., HOPKINS, R. H., MCMULLIN, P. G., CLARKE, R. C., & CHOYKE, W. J. Growth of large SiC single crystals. *J. Crystal Growth* **128** (1993), 358–362.
2. CARTER JR., C., TSVETKOV, V. F., GLASS, R. C., HENSHALL, D., BRADY, M., MÜLLER, ST. G., KORDINA, O., IRVINE, K., EDMOND, J. A., KONG, H.-S., SINGH, R., ALLEN, S. T., & PALMOUR, J. W. Progress in SiC: from material growth to commercial device development. *Mater. Sci. Eng. B* **61–62** (1999), 1–8.

3. CHEN,Q.-S., ZHANG, H., PRASAD, V., BALKAS, C. M., & YUSHIN, N. K. A system model for silicon carbide crystal growth by physical vapor transport method. *1999 National Heat Transfer Conference*, NHTC99-222, ASME (1999), 1–8.
4. CLAIN, S., RAPPAZ, J., & ŚWIERKOSZ, M. Coupling between nonlinear Maxwell and heat equations for an induction heating problem: Modeling and numerical methods. *Finite Element Methods. 50 Years of the Courant Element*, M. Křižek et al. (eds.), Lecture Notes Pure Appl. Math. 164, Dekker, New York (1994), 163–171. Zbl 0812.65122
5. DUPRET, F., NICODÈME, P., RYCKMANS, Y., WOUTERS, P., & CROCHET, M. J. Global modelling of heat transfer in crystal growth furnaces. *Int. J. Heat Mass Transfer* **33** (1990), 1849–1871. Zbl 0708.76126
6. FUHRMANN, J., KOPRUCKI, TH., & LANGMACH, H. pdelib: An open modular tool box for the numerical solution of partial differential equations. Design patterns. *Proc. 14th GAMM Seminar on Concepts of Numerical Software* (Kiel, 1998), Kiel (2001).
7. GLASS, R. C., HENSHALL, D., TSVETKOV, V. F., & CARTER JR., C. H. SiC seeded crystal growth. *Phys. Stat. Sol. (b)* **202** (1997), 149–162.
8. JÄRVINEN, J. *Mathematical Modeling and Numerical Simulation of Czochralski Silicon Crystal Growth*. PhD thesis, Univ. Jyväskylä, 1996.
9. KARPOV, S. YU., KULIK, A. V., ZHMAKIN, I. A., MAKAROV, YU. N., MOKHOV, E. N., RAMM, M. G., RAMM, M. S., ROENKOV, A. D., & VODAKOV, YU. A. Analysis of sublimation growth of bulk SiC crystals in tantalum container. *J. Crystal Growth* **211** (2000), 347–351.
10. KLEIN, O. & PHILIP, P. Correct voltage distribution for axisymmetric sinusoidal modeling of induction heating with prescribed current, voltage, or power. *IEEE Trans. Mag.* **38** (2002), 1519–1523.
11. KLEIN, O. & PHILIP, P. Transient numerical investigation of induction heating during sublimation growth of silicon carbide single crystals. *J. Crystal Growth* **247** (2003), 219–235.
12. KLEIN, O., PHILIP, P., SPREKELS, J., & WILMAŃSKI, K. Radiation- and convection-driven transient heat transfer during sublimation growth of silicon carbide single crystals. *J. Crystal Growth* **222** (2001), 832–851.
13. KONSTANTINOV, A. O. Sublimation growth of SiC. *Properties of Silicon Carbide*, G. Harris (ed.), EMIS Datareview Ser. 13, Institution of Electrical Engineers, INSPEC, London (1995), Ch. 8.2, 170–203.
14. MODEST, M. F. *Radiative Heat Transfer*. McGraw-Hill Ser. Mech. Eng., McGraw-Hill, New York (1993).
15. MÜLLER, ST. G., GLASS, R. C., HOBGOOD, H. M., TSVETKOV, V. F., BRADY, M., HENSHALL, D., MALTA, D., SINGH, R., PALMOUR, J., & CARTER JR., C. H. Progress in the industrial production of SiC substrates for semiconductor devices. *Mater. Sci. Eng. B* **80** (2001), 327–331.
16. PHILIP, P. *Transient Numerical Simulation of Sublimation Growth of SiC Bulk Single Crystals. Modeling, Finite Volume Method, Results*. PhD thesis, Dept. Math., Humboldt Univ. of Berlin (2003). Report No. 22, Weierstraß-Institut für Angewandte Analysis und Stochastik, Berlin. Zbl pre01974327
17. PONS, M., ANIKIN, M., CHOUROU, K., DEDULLE, J. M., MADAR, R., BLANQUET, E., PISCH, A., BERNARD, C., GROSSE, P., FAURE, C., BASSET, G., & GRANGE, Y. State of the art in the modelling of SiC sublimation growth. *Mater. Sci. Eng. B* **61–62** (1999), 18–28.
18. RAPPAZ, J. & ŚWIERKOSZ, M. Modelling in numerical simulation of electromagnetic heating. *Modelling and Optimization of Distributed Parameter Systems* (Warsaw, 1995), Chapman & Hall, New York (1996), 313–320. Zbl 0879.65091 MR 1388547
19. ROST, H.-J., SICHE, D., DOLLE, J., EISERBECK, W., MÜLLER, T., SCHULZ, D., WAGNER, G., & WOLLWEBER, J. Influence of different growth parameters and related conditions on 6H-SiC crystals grown by the modified Lely method. *Mater. Sci. Eng. B* **61–62** (1999), 68–72.
20. SCHULZE, N., BARRETT, D. L., & PENSL, G. Near-equilibrium growth of mircopipe-free 6H-SiC single crystals by physical vapor transport. *Appl. Phys. Lett.* **72** (1998), 1632–1634.

21. SEGAL, A. S., VOROB'EV, A. N., KARPOV, S. YU., MOKHOV, E. N., RAMM, M. G., RAMM, M. S., ROENKOV, A. D., VODAKOV, YU. A., & MAKAROV, YU. N. Growth of silicon carbide by sublimation sandwich method in the atmosphere of inert gas. *J. Crystal Growth* **208** (2000), 431–441.
22. SHEWCHUK, J. R. Triangle: Engineering a 2d quality mesh generator and Delaunay triangulator. *Applied Computational Geometry* (Philadelphia, PA, 1996), Lecture Notes in Comput. Sci. 1148, Springer (1998), 124–133.
23. SPARROW, E. M. & CESS, R. D. *Radiation Heat Transfer*. Hemisphere Publ. Corp., Washington, DC (1978).